Available online at www.sciencedirect.com
SCIENCE DIRECT®
Physics Letters A 344 (2005) 253–264
PHYSICS LETTERS A
www.elsevier.com/locate/pla

Multiplicative multifractal modeling and discrimination of human neuronal activity

Yi Zheng [a], Jianbo Gao [a,*], Justin C. Sanchez [a], Jose C. Principe [a], Michael S. Okun [b]

[a] *Department of Electrical and Computer Engineering, University of Florida, Gainesville, FL 32611, USA*
[b] *Department of Neurology, University of Florida, Gainesville, FL 32611, USA*

Received 6 January 2005; received in revised form 9 June 2005; accepted 14 June 2005

Available online 5 July 2005

Communicated by C.R. Doering

Abstract

Understanding neuronal firing patterns is one of the most important problems in theoretical neuroscience. It is also very important for clinical neurosurgery. In this Letter, we introduce a computational procedure to examine whether neuronal firing recordings could be characterized by cascade multiplicative multifractals. By analyzing raw recording data as well as generated spike train data from 3 patients collected in two brain areas, the globus pallidus externa (GPe) and the globus pallidus interna (GPi), we show that the neural firings are consistent with a multifractal process over certain time scale range (t_1, t_2), where t_1 is argued to be not smaller than the mean inter-spike-interval of neuronal firings, while t_2 may be related to the time that neuronal signals propagate in the major neural branching structures pertinent to GPi and GPe. The generalized dimension spectrum D_q effectively differentiates the two brain areas, both intra- and inter-patients. For distinguishing between GPe and GPi, it is further shown that the cascade model is more effective than the methods recently examined by Schiff et al. as well as the Fano factor analysis. Therefore, the methodology may be useful in developing computer aided tools to help clinicians perform precision neurosurgery in the operating room.

1. Introduction

Events in extracellular neuronal recording generate two types of time series: (1) the time interval between successive firings, called the inter-spike-interval (ISI) data; (2) a counting process, representing the number of firings in a chosen time window. In the past few decades, a lot of effort has been dedicated to the analysis of these two types of time series, by using fractal theory to characterize how firing data is different from Poisson-based models, to quantify long-range-correlations, and to characterize the neuronal dynamics [1–22]. Much new insights into the functional importance of multiscale spike train variabilities have been gained. In this Letter, we introduce a dif-

* Corresponding author.
E-mail address: gao@ece.ufl.edu (J. Gao).

0375-9601/$ – see front matter
doi:10.1016/j.physleta.2005.06.092

ferent type of fractal process, called a multiplicative cascade multifractal, for the analysis of neuronal firing patterns.

Neuronal firing patterns are also important in clinical neurosurgery. Advances in surgical treatment of Parkinson disease have stimulated much interest in the research of deep brain stimulation (DBS). The globus pallidus (GP) has been targeted in neurosurgical treatment of Parkinson disease and dystonia. The GP is a complex structure in the basal ganglia and can be divided into two parts: the globus pallidus externa (GPe) and the globus pallidus interna (GPi). Both receive input from the caudate and putamen and communicate with the subthalamic nucleus. The GPi is thought to send the major inhibitory output from the basal ganglia back to thalamus, and also to send a few projections to an area of midbrain (the PPPA), presumably to assist postural control. Distinguishing GPe from GPi is very important for surgical treatment of Parkinson disease [23].

In his pioneering work, DeLong [24] observed that discharge patterns of neurons in the GPi and GPe in awake monkey (*Macacca Mulatta*) at rest appeared to be very different. For GPe neurons, two types of firing patterns were observed: one had recurrent periods of high-frequency discharge with relatively silent periods in between, and the other had a low-frequency discharge with bursts. In contrast, only one firing pattern was found for GPi neurons: a continuously discharge without long periods of silence. DeLong's work makes one wonder whether different cell types in specific brain regions can be characterized and identified by their firing patterns, so that the accuracy in the target acquisition of stereotactic electrode placement in the human brain can be automated with high accuracy. Indeed, a lot of work has been done since then [25–30]. However, recently it was reported that traditional signal processing of single-unit neuronal activity may fail to differentiate GPe and GPi in Parkinson disease [28]. However, the negative result of [28] does not imply that single-unit neuronal activity recordings do not contain enough information for us to differentiate between GPe and GPi, because in practice, a well trained experienced movement disorders specialist is able to do so by listening to neuronal activity over a loudspeaker through trial and error. The success of movement disorders specialist and the importance of differentiating GPe and GPi in clinical neurosurgery motivates us to examine whether more advanced signal processing tools, such as those based on multifractal theory, may help us achieve this goal better.

The remaining of the Letter is organized as follows. We briefly describe the data in Section 2. In Section 3, we first overview measure based multifractal theory, and then briefly describe multiplicative cascade multifractals. In Section 4, we first describe a procedure to carry out multifractal analysis on experimental data, then we present a detailed analysis on human deep brain recording data as well as generated spike train data, and show that the neuronal activity data exhibits stochastic features that are consistent with the multiplicative cascade multifractal model. In particular, we show that the model appears to be able to distinguish GPe from GPi based on neuronal firing data analysis. For comparison purpose, we also study the data using Fano factor analysis and the methods recently examined by Schiff et al. [28]. We summarize our findings in the final section.

2. Data

We have obtained sequences of the neural activity from GPi and GPe of 3 patients, sampled at 20 kHz. The measured voltage recording data for three patients are shown in Fig. 1. In this Letter, we analyze both raw voltage recording data as well as spike train data. To appreciate the data better, a small representative segment is shown in Fig. 2. We observe two time scales: (i) the inter-spike-interval (ISI), which on average is about 0.01 s (i.e., around 200 sampled points) for both GPi and GPe; (ii) a smaller time scale defining each spike, which contains around 16 sampled points. For time scales below the average ISI, neural activity signals cannot be fractals; therefore, we expect that fractal analysis of neuronal firing patterns should involve time scales larger than the two time scales discussed above. This is indeed the case, as will be pointed out explicitly later.

The method we adopt for spike-detect is similar to that used by Schiff et al. [28]. The method contains 3 thresholds and consists of 3 steps: (1) starting from the center line (i.e., zero voltage), a threshold is used to identify a candidate spike peak; (2) starting from the identified candidate peak, a second threshold is used to identify a valley; (3) a slope is defined by connecting

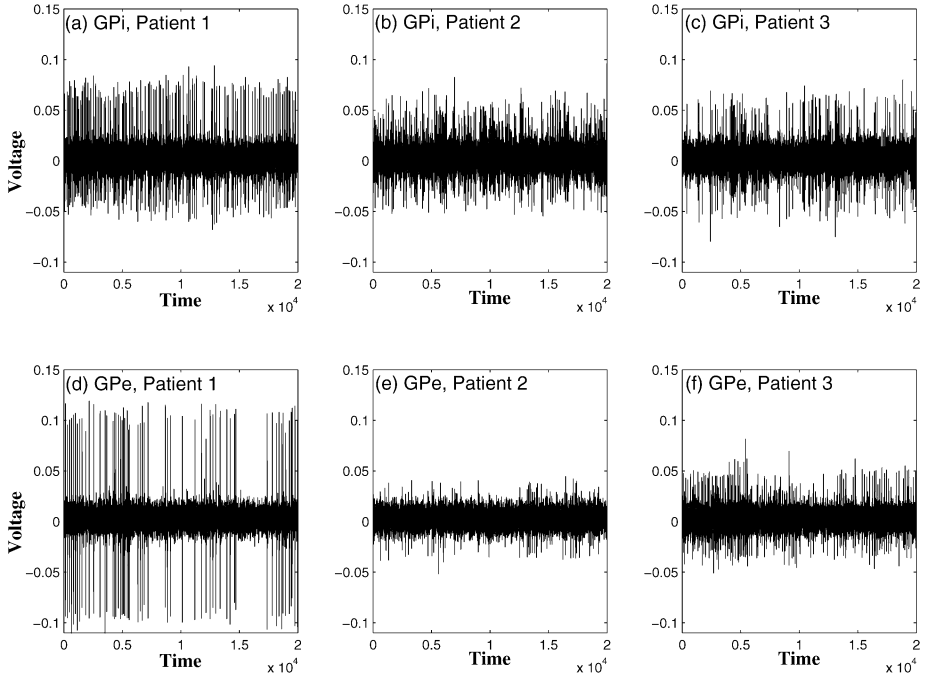

Fig. 1. Human deep brain recordings from GPe and GPi.

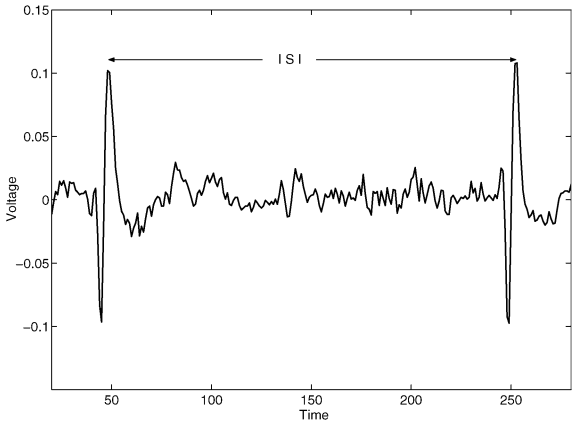

Fig. 2. Detailed neural discharge data.

the identified peak and valley. If the slope exceeds a third threshold, the identified spike is declared as a true spike.

From Fig. 1, we can see that the data sets of patient 1 are "cleaner" than data sets of other two patients. To quantify this visual perception, we define signal to noise ratio (SNR) by the formula $\mathrm{SNR} = 20\log_{10}(\frac{A}{\sigma})$, where A is the mean amplitude of the identified spike peaks, and σ is the standard deviation of the background noise. The latter is computed by first removing the identified spikes from the voltage data. The result is shown in Table 1. We observe that the SNR for the data of patient 1 is the highest. This is consistent with our earlier observation.

Table 1
SNR of recording data of 3 patients

Data	Patient 1		Patient 2		Patient 3	
	GPi	GPe	GPi	GPe	GPi	GPe
SNR	18.3	22.0	13.2	11.5	14.9	12.5

Finally, we note that the maximum ISI for GPi is about 0.06 s, and about 0.40 s for GPe. This suggests that neuronal firing in GPe may be more intermittent than that in GPi, which is consistent with DeLong's observation.

3. Multiplicative cascade multifractals

The concept of multifractal is mostly developed for understanding the intermittent features of turbu-

lence [31]. Intuitively, intermittency can be considered a combination of burstiness and the variation of the burstiness over time. In this section, we first overview the definition of measure based multifractals. This type of multifractals is typically constructed through multiplicative processes. In the following, we define multiplicative processes and present examples of such models.

3.1. Definition

Consider the unit interval, associate it with a unit mass, and partition the unit interval into a series of small intervals with linear length ϵ. Partition the unit mass into a series of weights or probabilities $\{w_i\}$, and associate w_i with the ith interval. Now consider the moments

$$M_q(\epsilon) = \sum_i w_i^q, \tag{1}$$

where q is real. Note the convention that whenever w_i is zero, the term w_i^q is dropped. We also note that a positive q value emphasizes large weights, while a negative q value emphasizes small weights. If we have, for a real function $\tau(q)$ of q,

$$M_q(\epsilon) \sim \epsilon^{\tau(q)}, \quad \text{as } \epsilon \to 0, \tag{2}$$

for every q, and the weights $\{w_i\}$ are non-uniform, then the weights $w_i(\epsilon)$ are said to form a multifractal measure. Note that the normalization $\sum_i w_i = 1$ implies that $\tau(1) = 0$.

Note that if $\{w_i\}$ are uniform, then $\tau(q)$ is linear in q. When $\{w_i\}$ are weakly non-uniform, visually $\tau(q)$ may still be approximately linear in q. The non-uniformity in $\{w_i\}$ is better characterized by the so-called generalized dimensions D_q defined as [32]

$$D_q = \frac{\tau(q)}{q-1}. \tag{3}$$

D_q is a monotonically decreasing function of q [33]. It exhibits a non-trivial dependence on q when the weights $\{w_i\}$ are non-uniform. We will use this property to distinguish the activity from two types of deep brain structures, the GPe and GPi.

3.2. Construction of multiplicative multifractals

To better appreciate the construction rules, we point out that they essentially involve dyadic partitions.

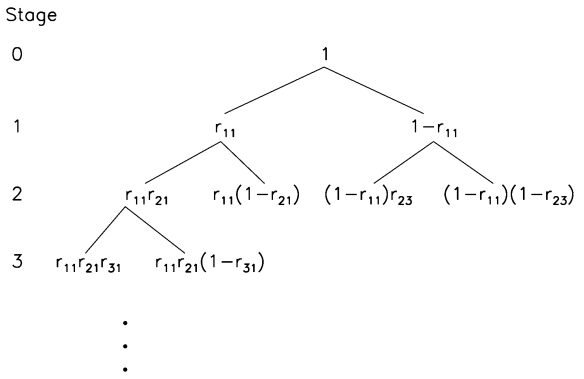

Fig. 3. Schematic illustrating the construction rule of a multiplicative multifractal.

Consider a unit interval again and associate it with a unit mass. Divide the unit interval into two, say, left and right segments of equal length. Also partition the associated mass into two fractions, r and $1-r$, and assign them to the left and right segments, respectively. The parameter r is in general a random variable, governed by a probability density function (pdf) $P(r)$, $0 \leqslant r \leqslant 1$. The fraction r is called the multiplier. Each new subinterval and its associated weight are further divided into two parts following the same rule. This procedure is schematically shown in Fig. 3, where the multiplier r is written as r_{ij}, with i indicating the stage number, and j (assuming only odd numbers thus leaving even numbers for $1 - r_{ij}$) indicating the positions of a weight on that stage. Note the scale (i.e., the interval length) associated with stage i is 2^{-i}. We assume that $P(r)$ is symmetric about $r = 1/2$, and has successive moments $\mu_1, \mu_2, \ldots$. Hence r_{ij} and $1 - r_{ij}$ both have marginal distribution $P(r)$. The weights at the stage N $\{w_n, n = 1, \ldots, 2^N\}$, can be expressed as

$$w_n = u_1 u_2 \cdots u_N,$$

where u_l, $l = 1, \ldots, N$, are either r_{ij} or $1 - r_{ij}$, thus, $\{u_i, i \geqslant 1\}$ are independent identically distributed random variables having pdf $P(r)$. One can readily prove that such a model generates multifractals [34]. To better appreciate the model and to develop a general analysis procedure, in the following, we illustrate this process by selecting a specific pdf $P(r)$.

Deterministic binomial multiplicative process

In this case, the pdf is set to be equal to $P(r) = \delta(r - p)$, where $\delta(x)$ is the Kronecker delta function.

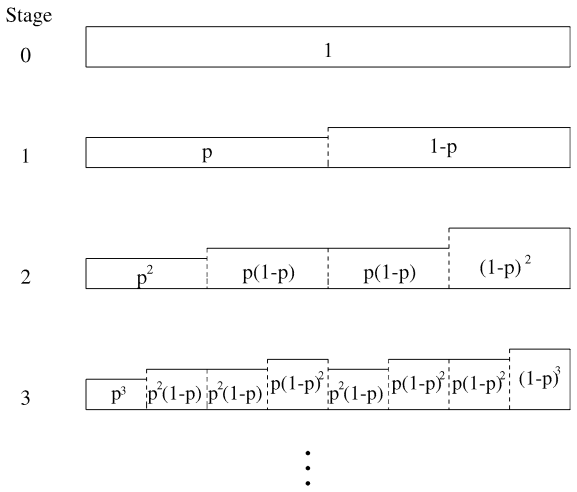

Fig. 4. A schematic showing the weights at the first several stages of the binomial multiplicative process ($r = p$ w.p. 1).

Thus, $r = p$ with probability 1, where $0 < p < 1$ is a fixed number. The weights obtained for the first several stages are schematically shown in Fig. 4.

For this process, at stage n, we have

$$M_q(\epsilon) = \sum_{i=0}^{n} C_n^i p^{qi}(1-p)^{q(n-i)} = \left[p^q + (1-p)^q\right]^n. \tag{4}$$

Since at stage n, $\epsilon = 2^{-n}$, we obtain

$$\tau(q) = -\ln\left[p^q + (1-p)^q\right]/\ln 2, \tag{5}$$

which is independent of n (or ϵ). Hence, this weight process constitutes a multifractal [35,36].

Random binomial multiplicative process

To make the weight series random, we can select the function $P(r)$ in any functional form [33], as long as $P(r)$ is symmetric about $r = 1/2$. One of the simplest cases is the random binomial multiplicative process, where $P(r)$ is given by

$$P(r) = \left[\delta(r-p) + \delta\big(r-(1-p)\big)\right]/2. \tag{6}$$

It is quite obvious that the $\tau(q)$ spectrum for this process is identical to that for the deterministic binomial process, since the weight sequence for this process is simply a shuffled version of the deterministic case.

4. Analysis of experimental data

In this section, we apply multiplicative multifractal analysis to human deep brain recording data as well as generated spike train data. We show that human deep brain neuronal activity data exhibit stochastic features that are consistent with the stochastic behavior of random multiplicative processes over certain time scales, and these features can be used to distinguish neurons from GPe and GPi. For comparison purpose, we also study the data using Fano factor analysis and the methods recently proposed by Schiff et al. [28].

4.1. Multiplicative multifractal analysis of raw recording data

In order to show that the data recorded in different brain areas are realizations of certain multiplicative processes, moments $M_q(\epsilon)$ are computed at different stages, and Eq. (2) is checked for validity in certain ϵ ranges. In the following, we describe in detail a general procedure for obtaining weight sequences at different stages needed for computing the moments $M_q(\epsilon)$.

Assume we use 2^N consecutive raw recording voltage data. For ease of illustration, we denote this original time series as $\{V_i\}$; and the square of raw data, $\{V_i^2\}$, by $\{X_i\}$. We view $\{X_i, i = 1, \ldots, 2^N\}$ as the weight series of a certain multiplicative process at stage N. Note that the total weight $\sum_{i=1}^{2^N} X_i$ is set equal to 1 unit. Also note the scale associated with stage N is $\epsilon = 2^{-N}$. This is the smallest time scale resolvable by the measured human deep brain recording data.

Given the weight sequence at stage N (which represents the measured data), the weights at stage $N-1$, $\{X_i^{(2^1)}, i = 1, \ldots, 2^{N-1}\}$, is obtained by simply adding the consecutive weights at stage N over non-overlapping blocks of size 2, i.e., $X_i^{(2^1)} = X_{2i-1} + X_{2i}$, for $i = 1, \ldots, 2^{N-1}$, where the superscript 2^1 for $X_i^{(2^1)}$ is used to indicate that the block size used for the involved summation at stage $N-1$ is 2^1. This follows directly from the construction of a multiplicative multifractal process, as schematized in Fig. 3. Associated with this stage is the scale $\epsilon = 2^{-(N-1)}$. This procedure is carried out recursively. That is, given the weights at stage $j+1$,

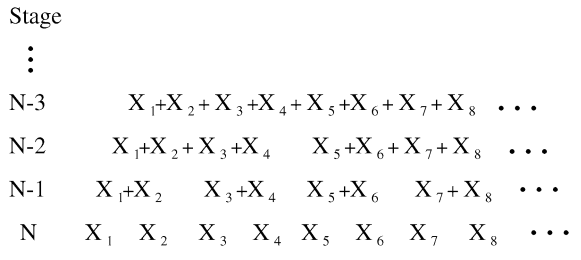

Fig. 5. A schematic showing the weights at the last several stages for the analysis procedure described in the text. It is instructive to compare this figure with Fig. 3, where it was shown that a weight at stage i is the sum of the two "daughter" weights at stages $i+1$.

$\{X_i^{(2^{N-j-1})}, i = 1, \ldots, 2^{j+1}\}$, we obtain the weights at stage j, $\{X_i^{(2^{N-j})}, i = 1, \ldots, 2^j\}$, by adding consecutive weights at stage $j+1$ over non-overlapping blocks of size 2, i.e.,

$$X_i^{(2^{N-j})} = X_{2i-1}^{(2^{N-j-1})} + X_{2i}^{(2^{N-j-1})}, \tag{7}$$

for $i = 1, \ldots, 2^j$. Here the superscript 2^{N-j} for $X_i^{(2^{N-j})}$ is used to indicate that the weights at stage j can be equivalently obtained by adding consecutive weights at stage N over non-overlapping blocks of size 2^{N-j}. Associated with stage j is the scale $\epsilon = 2^{-j}$. This procedure stops at stage 0, where we have a single unit weight, $\sum_{i=1}^{2^N} X_i$, and $\epsilon = 2^0$. The latter is the largest time scale associated with the measured neural data. Fig. 5 schematically shows this procedure.

After we have obtained all the weights from stages 0 to N, we compute the moments $M_q(\epsilon)$ according to Eq. (1) for different values of q. We then plot $\log M_q(\epsilon)$ vs. $\log \epsilon$ for different values of q. If these curves are linear over a wide range of ϵ, then these weights are consistent with a multifractal measure. Note that, according to Eq. (2), the slopes of the linear part of $\log M_q(\epsilon)$ vs. $\log \epsilon$ curves provide an estimate of $\tau(q)$, for different values of q.

We illustrate the above procedure by using 2^{17} consecutive data points of each data set for this analysis, which is around 6.5 seconds. To assess the degree of linearity we plot in Fig. 6 $\log_2 M_q(\epsilon)$ vs. $-\log_2 \epsilon$ for voltage data recorded from GPi and GPe of all three patients. We observe that the scaling between $M_q(\epsilon)$ and ϵ (i.e., the degree of linearity between $\log_2 M_q(\epsilon)$ and $-\log_2 \epsilon$) for all data sets are quite good up to the 9th stage.

To further check whether these data sets are truly multifractals, we compute D_q for certain ϵ range. Here we focus on the time scale range from stage 9 to stage 4, corresponding to time scales from about $t_1 = 0.01$ to $t_2 = 0.40$ s (more precisely, 2^{17-9} and 2^{17-4} sampled points, with a sampling frequency of 20 kHz). The results are shown in Fig. 7. Indeed we observe that in all cases D_q has a nontrivial dependence on q. Therefore, we conclude that these time series are consistent with multifractals.

More interestingly, the D_q spectrum shows clearly the difference between the neuronal firings in GPe and GPi. This is evident from Fig. 7 where we observe that there is a clear separation between the values of D_q at very negative values of q (say, $q = -30$) for GPi and GPe ($D_q \sim 1.4$ for GPi and ~ 1.2 for GPe). This result can be understood readily. The small intervals with smaller weight will dominate the moments of M_q when q is very negative. For time scales just exceeding the mean ISI, which corresponding to about $\epsilon = 2^8$ points, some intervals may not contain any neuronal firing and thus will weigh a lot more for very negative q. As noted before, for GPi, the discharge is fairly uniform, while for GPe, the firings are more bursty and intermittent, and hence may result in many long time intervals without any firing. As a consequence, for very negative q, M_q for GPe decays slower than that for GPi, and hence, a smaller D_q. Therefore, the D_q spectrum provides an interesting means of quantifying the structures of ISI as well as the differences between the firing patterns of the neurons in GPe and GPi.

We emphasize that based on our analysis of three patients' data, the separation between GPe and GPi based on the D_q, $q < 0$, curves holds not only for the same patient, but also across patients. The values of D_q were consistent among the three patients which settled to ~ 1.4 for GPi and ~ 1.2 for GPe. This result warrants a more rigorous study involving a much larger patient population to verify these trends.

4.2. Multiplicative multifractal analysis of spike train data

We now apply the multiplicative multifractal analysis to the spike train data. To do so, we represent the

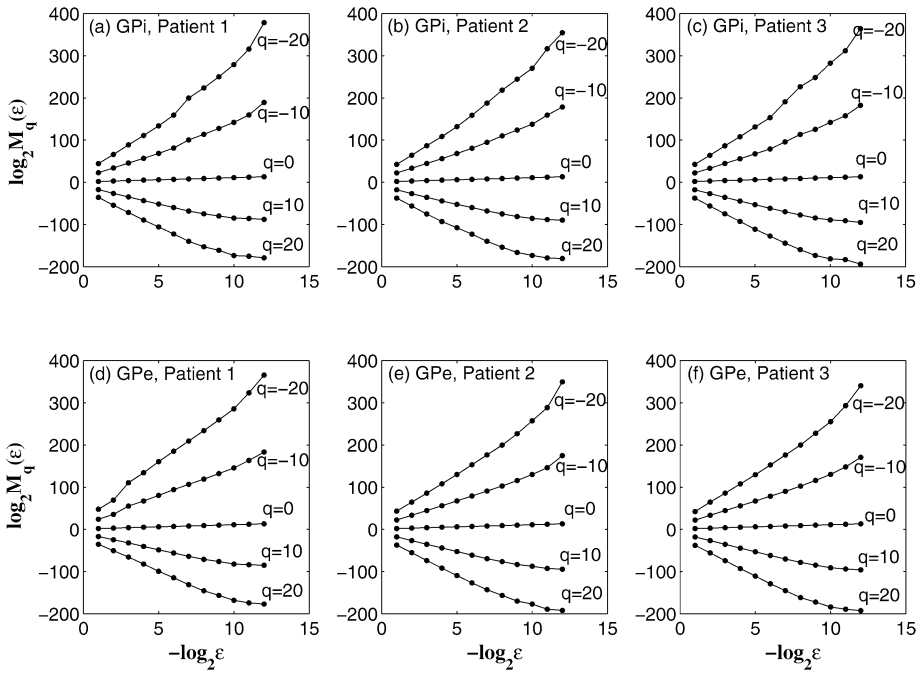

Fig. 6. $\log_2 M_q(\epsilon)$ vs. $-\log_2 \epsilon$ for human brain deep recordings for several different q's.

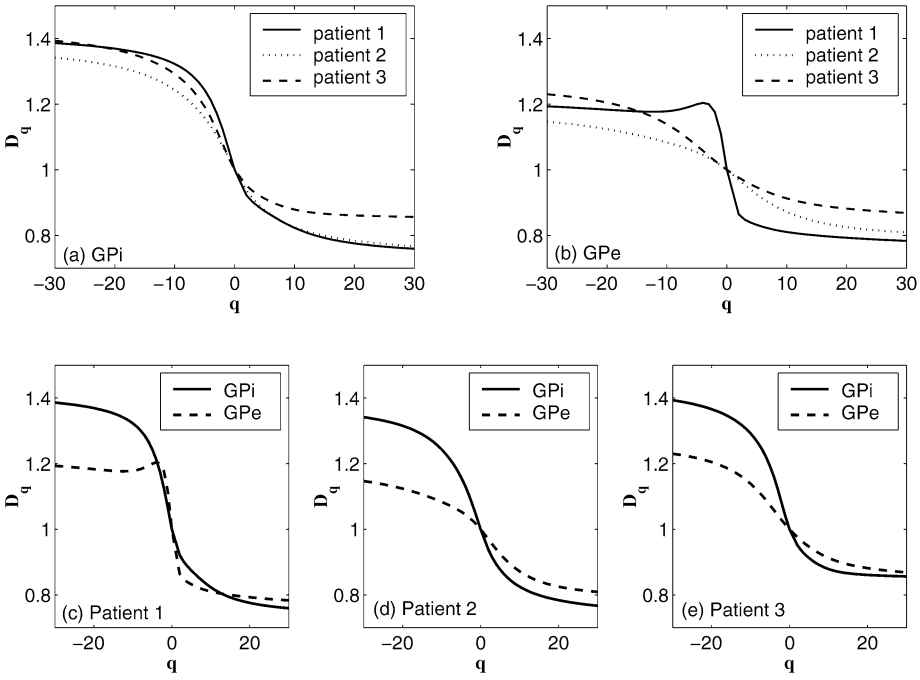

Fig. 7. The generalized dimension spectrum for recording data of GPi and GPe area of 3 patients.

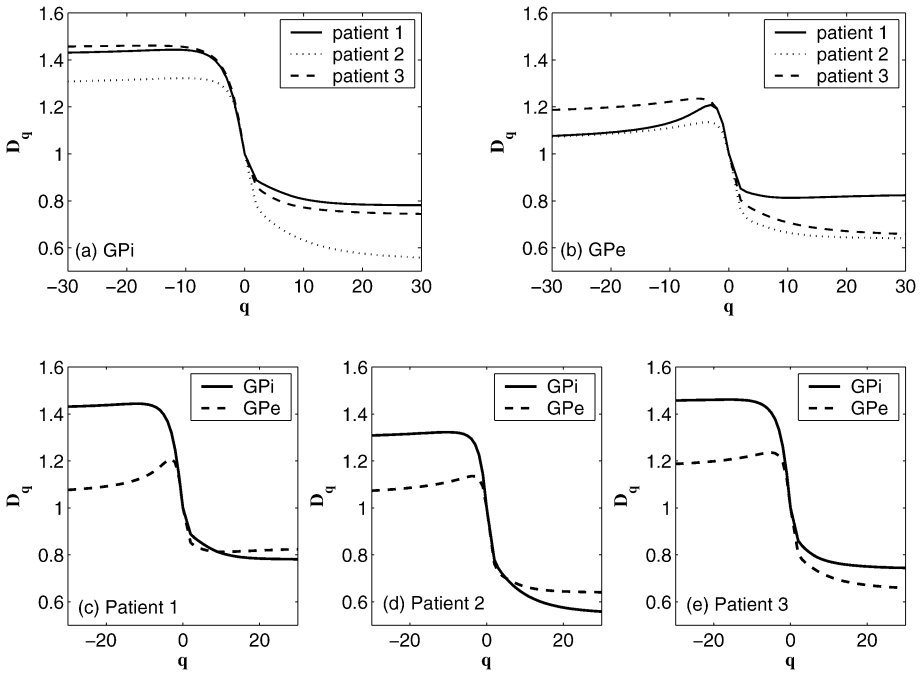

Fig. 8. The generalized dimension spectrum for spike train data of GPi and GPe area of 3 patients. The spike trains are obtained under one set of threshold values.

spike train data by the following: we set $X_i = 1$ when there is a spike at the position i, and more or less arbitrarily set $X_i = 0.001$ when there is no spike at the position i. After obtaining such a time series, we then apply the general analysis procedure discussed above to obtain the generalized dimension spectrum D_q. Very interestingly, the time scale region defining the fractal scaling here is the same as that identified earlier, i.e., from $t_1 = 0.01$ to about $t_2 = 0.4$ s. Fig. 8 shows the result for the spike train data under one set of threshold values used for obtaining the spikes. Comparing with Fig. 7, we observe that the differences between the D_q, $q < 0$, curves, for GPe and GPi become even larger for the spike train data than for the raw data, especially for the data of patient 1, which is cleanest.

We have further examined how sensitively the result of Fig. 8 depends on the threshold values used for spike detection. We have found that when the data is clean, the sequence of the spikes detected is largely independent of the threshold values. So are the D_q curves. This is evident by comparing Fig. 9(c) with Fig. 8(c), where the spike train for Fig. 9(c) is obtained with a set of smaller threshold values. However, when the data is very noisy, the sequence of spikes detected can be drastically modified by the threshold values. As a result, the D_q curves shift upward, sometimes quite significantly, when the threshold values used for detecting the spikes are reduced. This can be clearly seen by comparing Fig. 9(d), (e) with Fig. 8(d), (e). While Fig. 8 indicates that the multifractal model becomes more effective in differentiating GPe from GPi when employed to analyze spike data, Fig. 9 says the opposite.

Our results can be understood readily. When the data is clean, spike detection effectively suppresses noise. Consequently, the multifractal model becomes more effective in distinguishing between GPe and GPi. However, when data is not very clean, spike detection both suppresses and introduces noise. The former comes from the fact that noise between spikes has been completely removed, while the latter is due to the fact that spike detection may miss some true spikes while introduce some false spikes. As a result, the multifractal approach could become less effective when distinguishing GPe from GPi.

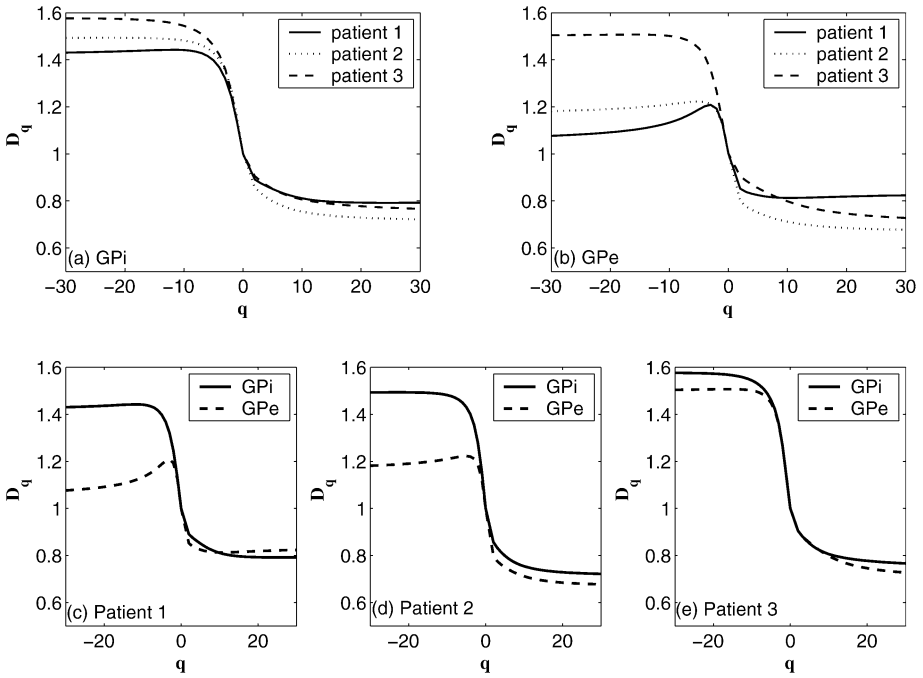

Fig. 9. The generalized dimension spectrum for spike train data of GPi and GPe area of 3 patients. The spike trains are obtained with threshold values that are smaller than those used in Fig. 8.

4.3. Comparison with other methods

In this subsection, we examine effectiveness of the methods studied in [28] as well as the Fano factor analysis in differentiating GPe from GPi.

Schiff et al. [28] examined the effectiveness of three simple measures for the analysis of single-unit neuronal recording to differentiate the GPi from GPe in Parkinson disease. The three measures are: (i) the mean firing frequency, which is simply the average spike firing rate; (ii) the burst firing ratio of spikes, which is defined as the percentage of ISIs that are shorter than 8 ms; and (iii) total average power of raw data, which is obtained by first computing the power spectrum within all 0.2048-second windows, and then getting the average. Table 2 lists our results. We observe that none of the measures works at all in distinguishing between GPe and GPi, just as reported by Schiff et al. [28].

Next we analyze neural firing activities by employing Fano factor analysis. The Fano factor is defined as

$$F(T) = \frac{\mathrm{Var}[N_i(T)]}{\mathrm{Mean}[N_i(T)]}, \tag{8}$$

Table 2
Comparison of mean firing frequency (Hz), bursts (percentage of ISI < 8 ms), and average power from raw data of 3 patients

Measurement	Patient 1		Patient 2		Patient 3	
	GPi	GPe	GPi	GPe	GPi	GPe
Mean freq.	95	71	101	51	139	135
Bursts (percent)	39.3	44.9	53.7	35.2	69.7	68.7
Average power	4.7	5.3	4.0	1.6	5.3	1.9

where $N_i(T)$ is the number of spikes in the ith window of duration T. For a Poisson process, $F(T)$ is 1, independent of T. For a fractal process, $F(T)$ not only depends on T, but the dependence takes on a power-law form: $F(T) \sim T^{2H-1}$, where H is called the Hurst parameter (or Holder exponent) [1,7]. Such a scaling can be readily understood, if one notices that for a fractal process such as fractional Brownian motion process, $\mathrm{Var}[N_i(T)] \sim T^{2H}$ [37].

In Fig. 10, we plot the $F(T)$ vs. T curves for all data sets in log–log scale. For short counting time ($T \to 0$), the Fano factors approach unity, because there is only zero or one spike in an arbitrarily short counting window and such a 0 and 1 counting se-

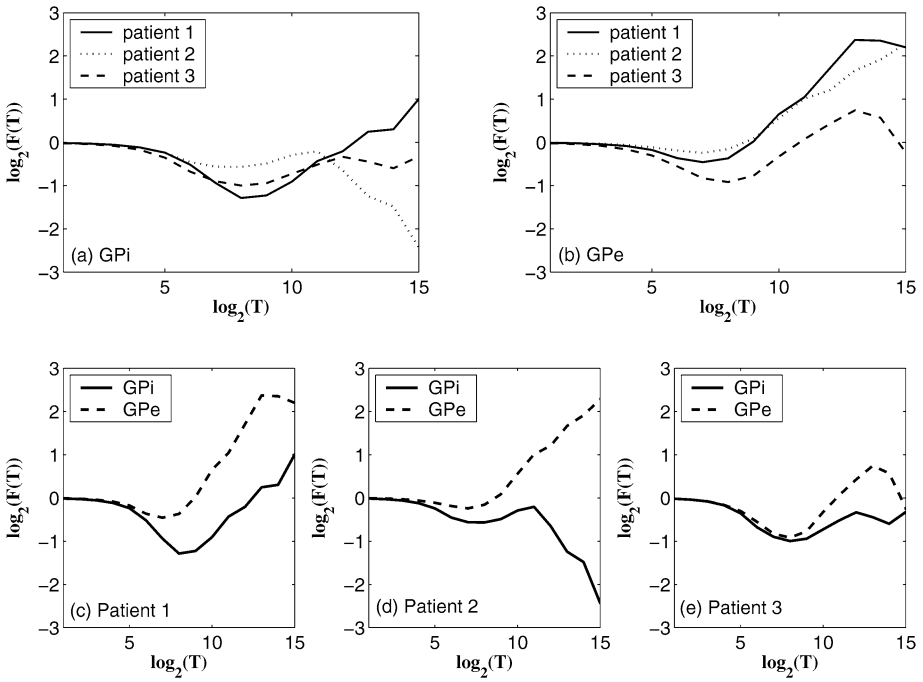

Fig. 10. $\log_2(F(T))$ vs. $\log_2(T)$ for spike train data of GPi and GPe area of 3 patients. The spikes are the same as those used in Fig. 8.

quence of spikes is a sequence of Bernoulli random variables [7]. When $T \geqslant 2^8$, which is equivalent to the mean of the ISI, for each patient, the $F(T)$ curve for GPe is higher than that for GPi. Therefore, the Fano factor appears to be able to distinguish GPe from GPi for individual patient, although not as effective as the multifractal model.

We would like to mention that we have also tried Fano factor analysis on the raw recording data. We are not able to identify any meaningful fractal scaling region, let alone to distinguish GPe from GPi.

5. Discussion

We have introduced a computational procedure to examine whether neuronal firing data could be characterized by cascade multiplicative multifractals. By studying short time series of duration 6.5 s, from 3 patients recorded in two brain structures, GPe and GPi, we have shown that the data are consistent with such multifractals over certain time scale range, and that the generalized dimension spectrum D_q accurately differentiates the two brain areas, both intra- and inter-patients. In so far as distinguishing GPe and GPi is concerned, it is found that the multifractal model is more effective than both conventional methods recently examined by Schiff et al. [28] as well as the Fano factor analysis. It is interesting to note that, by trial and error, a well trained experienced motion disorders specialist could discriminate the two brain areas in seconds to half minute. Therefore, the multifractal method may be very useful in helping develop quantitative methods to advise clinicians during precision neurosurgery in the operating room.

We have found that applying the multifractal analysis directly on the raw neural discharge data appears to be very effective in differentiating GPe and GPi, regardless of the degree of noise level in the data. This is because the analysis has built in it a simple mechanism—summation—to greatly suppress noise in the raw signals. This attribute is very appealing noticing that spike detection and sorting can be extremely complicated if the raw recording data is very noisy. Of course, if the raw recording data is very clean, then it would be better to perform spike detection first, to further reduce noise, before one employs the multiplicative multifractal analysis.

In our data sets we found that there are three time scales. One is the small time scale below the mean ISI of about 0.01 s. We have pointed out in Section 2 that on time scales smaller than the mean ISI, there is only noise and individual spikes, hence, fractal behavior should not be expected. We have also observed that, although the scaling behavior for the first 4 stages (corresponding to time scales of about 0.4 to 3 s) are consistent with a multifractal structure, they are not useful for the purpose of distinguishing between GPe and GPi. The time scale between 0.01 and 0.4 s is the one that contains the discriminating power for our goal. We have analyzed time series that are much longer than 2^{17} points, and observed similar behavior. Therefore, we have good reason to believe that distinguishing GPe from GPi may no longer be possible for time scales beyond 0.4 s. This may reflect properties of the physiological mechanisms that generate the data.

The notion of time scales can help us understand why some conventional measures are not effective in distinguishing GPe from GPi. To illustrate the point, let us consider why the total average power of raw data may fail to differentiate GPe from GPi. It is easy to understand that power spectral density has three contributions: (i) noise between spikes, (ii) shape of individual spikes, and (iii) the spacing between spikes. Presumably, only contribution from (iii) would be useful for the discrimination of GPe and GPi. Unfortunately, the contribution from (iii) has to be much less significant than those from (i) and (ii). It is thus clear that total average power of raw data cannot be effective in discriminating GPe from GPi.

The cascade multifractal model can be linked to the cytoarchitecture of the brain. We hypothesize that the ISI patterns at different time scales are related to the local and global neuronal interconnectivity. Since the propagation of neural signals is finite, time scales of ISI may reflect local and progressively longer neighborhoods of neural interaction, within and outside a given brain area. The smallest time scale defining each spike might only involve neural signal propagation within a cell assembly, and hence, not related to the fractal behavior. In fact, we have pointed out in Section 2 that fractal analysis has to involve time scales not smaller than the mean ISI. On the other hand, time scale longer than about 0.4 s might already correspond to neural interactions beyond GPi and GPe, hence, also irrelevant to distinguish among the two structures. These might explain why only the intermediate time scale is useful for discriminating between GPe and GPi.

Our proposed methodology produced a consistently quantifiable difference in the time-series recording between GPe and GPi within and across patients. Our ultimate goal is to develop an intra-operative advising system that generalizes to a much larger patient population and could be used to speedily and accurately confirm DBS targets. This approach could improve the success of DBS cases by decreasing intra-operative time, improving targeting, and easing the burden of classification by the movement disorder specialist. However, these results are simply a proof of concept and additional studies are necessary to confirm whether the observed multifractal trends are universal.

References

[1] M.C. Teich, IEEE Trans. Biomed. Engrg. 36 (1989) 150.
[2] S.B. Lowen, M.C. Teich, J. Acoust. Soc. Am. 92 (1992) 803.
[3] M.C. Teich, S.B. Lowen, IEEE Engrg. Med. Biol. Mag. 13 (2) (1994) 197.
[4] R.G. Turcott, S.B. Lowen, E. Li, D.H. Johnson, C. Tsuchitani, M.C. Teich, Biol. Cybern. 70 (3) (1994) 209.
[5] R.G. Turcott, P.D.R. Barker, M.C. Teich, J. Stat. Comput. Sim. 52 (3) (1995) 253.
[6] M.C. Teich, R.G. Turcott, R.M. Siegel, IEEE Engrg. Med. Biol. Mag. 15 (5) (1996) 79.
[7] M.C. Teich, C. Heneghan, S.B. Lowen, Y. Ozaki, E. Kaplan, J. Opt. Soc. Am. A 14 (1997) 529.
[8] S.B. Lowen, Phys. Rev. E 59 (5) (1999) 5970.
[9] A.R. Kumar, D.H. Johnson, J. Acoust. Soc. Am. 93 (6) (1993) 3365.
[10] R. Baddeley, L.F. Abbott, M.C. Booth, F. Sengpiel, T. Freeman, E.A. Wakeman, E.T. Rolls, Proc. R. Soc. London B 264 (1389) (1997) 1775.
[11] C.D. Lewis, G.L. Gebber, P.D. Larsen, S.M. Barman, J. Neurophysiol. 85 (4) (2001) 1614.
[12] M. Das, G.L. Gebber, S.M. Barman, C.D. Lewis, J. Neurophysiol. 89 (2) (2003) 833.
[13] R. Ratnam, M.E. Nelson, J. Neurosci. 120 (17) (2000) 6672.
[14] H.S. Orer, M. Das, S.M. Barman, G.L. Gebber, J. Neurophysiol. 90 (1) (2003) 47.
[15] S. Bahar, J.W. Kantelhardt, A. Neiman, H.H.A. Rego, D.F. Russell, L. Wilkens, A. Bunde, F. Moss, Europhys. Lett. 56 (3) (2001) 454.
[16] C. Koch, Biophysics of Computation, Oxford Univ. Press, New York, 1999.
[17] G.J. Ortega, M. Bongard, E. Louis, E. Fernndez, J. Neurosci. Methods 133 (2004) 135.

[18] S. Blesić, S. Milošević, D. Stratimirović, M. Ljubisavljević, Physica A 268 (1999) 275.
[19] J.W. Middleton, M.J. Chacron, B. Lindner, A. Longtin, Phys. Rev. E 68 (2) (2003) 021920.
[20] M.E. Nelson, J. Physiol. (Paris) 96 (5–6) (2002) 507.
[21] S. Blesić, S. Milošević, D. Stratimirović, M. Ljubisavljević, Physica A 330 (3–4) (2003) 391.
[22] D. Stratimirović, S. Milošević, S. Blesić, M. Ljubisavljević, Physica A 291 (2001) 13.
[23] J.L. Vitek, R.A. Bakay, T. Hashimoto, Y. Kaneoke, K. Mewes, J.Y. Zhang, D. Rye, P. Starr, M. Baron, R. Turner, M.R. DeLong, J. Neurosurgery 88 (1998) 1027.
[24] M.R. DeLong, J. Neurophysiol. 34 (1971) 414.
[25] R.A. Santiago, J. McNames, K. Burchiel, G.G. Lendaris, Neural Networks 16 (5–6) (2003) 601.
[26] D. Sterio, M. Zonenshayn, A.Y. Mogilner, A.R. Rezai, K. Kiprovski, P.J. Kelly, A. Beric, Neurosurgery 50 (1) (2002) 58, Discussion 67-9.
[27] E. Micheli-Tzanakou, P. Wojnicki, J. Hamilton, Neuronal signal processing in Parkinson's disease, International Joint Conference on Neural Networks, Hawaii, USA, 2002.
[28] S.J. Schiff, B.K. Dunagan, R.M. Worth, J. Neurosurgery 97 (2002) 119.
[29] R.L. Alterman, D. Sterio, A. Beric, P.J. Kelly, Neurosurgery 44 (2) (1999) 315.
[30] W.D. Hutchison, A.M. Lozano, R.R. Tasker, A.E. Lang, J.O. Dostrovsky, Exp. Brain Res. 113 (3) (1997) 557.
[31] U. Frisch, Turbulence—The Legacy of A.N. Kolmogorov, Cambridge Univ. Press, Cambridge, 1995.
[32] H.G.E. Hentschel, I. Procaccia, Physica D 8 (1983) 435.
[33] J.F. Gouyet, Physics and Fractal Structures, Springer, New York, 1995.
[34] J.B. Gao, I. Rubin, Electronics Lett. 36 (2000) 101.
[35] J.B. Gao, I. Rubin, Comput. Commun. 24 (2001) 1400.
[36] J.B. Gao, I. Rubin, Int. J. Commun. Syst. 14 (2001) 783.
[37] M.S. Taqqu, V. Teverovsky, Fractals 3 (1995) 785.